

Oishen Zhao

Walker Department of Mechanical Engineering, University of Texas at Austin, 204 E. Dean Keeton St., Austin, TX 78712 e-mail: qishenzhao0904@utexas.edu

Nan Hong

Walker Department of Mechanical Engineering, University of Texas at Austin, 204 E. Dean Keeton St., Austin, TX 78712 e-mail: nan1995@utexas.edu

Dongmei Chen

Walker Department of Mechanical Engineering,
University of Texas at Austin,
204 E. Dean Keeton St.,
Austin, TX 78712
e-mail: dmchen@me.utexas.edu

Wei Li

Walker Department of Mechanical Engineering,
University of Texas at Austin,
204 E. Dean Keeton St.,
Austin, TX 78712
e-mail: weiwli@austin.utexas.edu

A Dynamic System Model for Roll-to-Roll Dry Transfer of Two-Dimensional Materials and Printed Electronics

Roll-to-roll (R2R) dry transfer is an important process for manufacturing of large-scale two-dimensional (2D) materials and printed flexible electronics. Existing research has demonstrated the feasibility of dry transfer of 2D materials in a roll-to-roll setting with mechanical peeling. However, the process presents a significant challenge to system control due to the lack of understanding of the mechanical peeling behavior and the complexity of the nonlinear system dynamics. In this study, an R2R peeling process model is developed to understand the dynamic interaction among the peeling process parameters, including adhesion energy, peeling force, angle, and speed. Both simulation and experimental studies are conducted to validate the model. It is shown that the dynamic system model can capture the transient behavior of the R2R mechanical peeling process and be used for the process analysis and control design. [DOI: 10.1115/1.4054187]

1 Introduction

Roll-to-roll (R2R) manufacturing is emerging as a leading method for low-cost, high-throughput production of flexible electronics [1-4], organic solar cells [5-7], battery and fuel cell electrodes [8,9], and other system-in-foil-devices [10]. As the technology develops, mechanical peeling is becoming an important process to transfer thin film materials such as graphene and printed electronic features from one substrate to another to fabricate more sophisticated devices [11-14]. Large-scale graphene has been grown on metal substrates such as copper and nickel foils using chemical vapor deposition (CVD) [15-23]. After the growth, CVD graphene needs to be transferred to a target substrate such as polymer film to manufacture flexible and stretchable electronics. There are wet-chemical-based methods for R2R graphene transfer, including chemical etching [19,24] and electrochemical delamination [25,26]. However, these methods are undesirable for large-scale production, because they would generate a large amount of chemical waste and leave chemical residues that will alter the properties of the transferred material. In addition, the wet-chemical etching method does not allow the reuse of the graphene growth substrate, as it will need to be etched away. The method adds additional material cost to the manufacturing process.

Recently, an R2R dry transfer process was developed for twodimensional (2D) materials manufacturing using mechanical peeling [27,28]. The same process can be used in printed electronics to transfer separately fabricated patterns from one substrate to another for device integration. Figure 1 shows an illustration of the mechanical peeling process. The donor and receiver substrates are first laminated and loaded on the unwinding roller. The laminate is then fed into the peeling system and separated with two guiding rollers at the peeling front. After peeling, the 2D material or fabricated patterns from the donor substrate are transferred to the receiver substrate, and the two substrates are each collected with a rewinding roller. The peeling forces are provided by the rewinding rollers. Tension rollers are used to measure the tension forces in the web sections before and after peeling. The R2R mechanical peeling process is complex due to many factors, such as the properties of the flexible substrates, the rate-dependent adhesion energy, and coupled effects of peeling tension and web speed. Studies have shown that controlling the peeling process is critical to achieving successful pattern transfer for printed electronics [29]. It has also been shown that the peeling speed and tension force are important to ensure the quality of transferred 2D materials [30].

Mechanical peeling has been actively studied in the past [31–41]. Most previous studies only focused on steady-state behaviors with a setup where a soft layer of material is peeled from a rigid flat surface. Kendall [31] proposed an energy balance method to determine the force requirement for peeling thin films

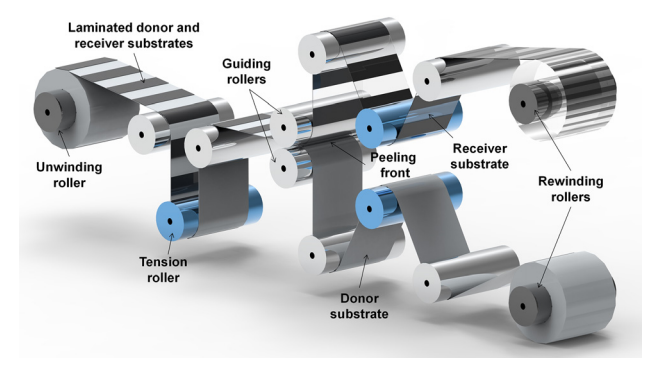


Fig. 1 An illustration of the R2R mechanical peeling process

¹Corresponding author.

Contributed by the Dynamic Systems Division of ASME for publication in the JOURNAL OF DYNAMIC SYSTEMS, MEASUREMENT, AND CONTROL. Manuscript received September 13, 2021; final manuscript received March 21, 2022; published online April 22, 2022. Assoc. Editor: David Hoelzle.

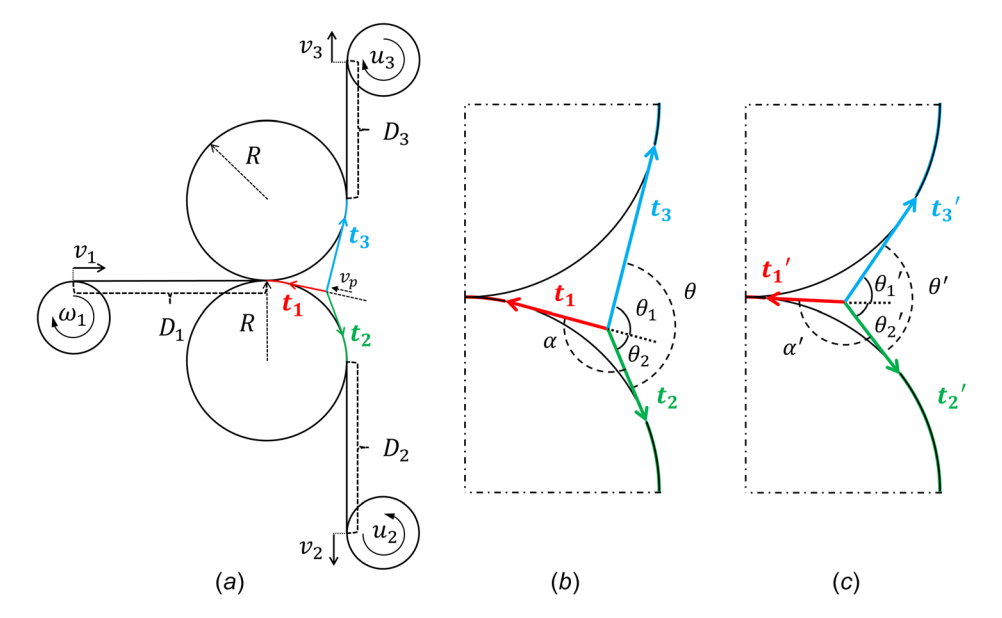


Fig. 2 (a) A schematic of the R2R peeling system. (b) and (c) Enlarged views of the peeling front with peeling angles shown. (b) and (c) also show that the peeling front location and peeling angles can change under different loading conditions.

from a rigid surface. Gao et al. [32] presented a theoretical analysis and simulation for the transfer behavior of 2D materials. Huang et al. [33] studied an R2R transfer printing process, with a focus on the steady-state delamination mechanics using a beam bending model. Wie et al. [34] reported the relationship between the steady-state peeling force and peeling angle in a wafer-scale batch transfer printing process. Yoo et al. [35] studied an adhesive stamp method for transfer-printing of semiconductor thin film patterns and found that the normal adhesion force depended on the stamp retraction angle. Many other studies focused on establishing the functional relationship between adhesion energy and peeling force, angle, and rate [36-39]. In addition, Dalbe et al. [40] investigated the stick-slip phenomenon during the peeling of pressure sensitive adhesives (PSA). Villey et al. [41] studied the ratedependent elastic hysteresis phenomenon in another PSA peeling process. Previous studies suggested that an optimal combination of peeling angles and peeling rate should be maintained to achieve successful transfer printing. However, none of them investigated the dynamics of the peeling process, let alone with an R2R configuration.

In this study, a dynamic R2R mechanical peeling model is developed for dry transfer of 2D materials and printed electronics. The model integrates the peeling front characteristics with roller dynamics of the web handling system to reveal the dynamic interaction among peeling process parameters, including adhesion energy, peeling force, angle, web speed, and peeling front velocity. The developed model is analyzed and validated with experimental data from a custom-built R2R mechanical peeling testbed. It provides important understanding of the R2R mechanical peeling process and can be used for advanced control algorithm design.

2 Modeling of Roll-to-Roll Mechanical Peeling Process

Figure 2(a) shows a schematic of the R2R mechanical peeling system. The system is actuated by three motors: a speed-controlled motor actuating the unwinding roller with the rotational speed denoted as ω_1 and two torque-controlled motors actuating the two rewinding rollers with torques u_2 and u_3 , respectively. The total web lengths from the unwinding and winding rollers to the corresponding tangential points of the two guiding rollers are defined as D_1 , D_2 , and D_3 . Before the peeling point, the laminate

is subject to tension t_1 , and after peeling, the peeled substrates are subject to tensions t_2 and t_3 , respectively. As shown in Fig. 2(b), the peeling angle between t_2 and t_3 is denoted as θ , and that between t_1 and t_2 is denoted as α . Angle θ can further be divided into θ_1 and θ_2 by the extension line of t_1 . Figure 2(c) shows that the peeling front location and peeling angles can change under a different loading condition.

At steady-state, the position of the peeling front is maintained at a fixed location to ensure a stable peeling process, where the peeling front propagates at a constant velocity v_p relative to the peeled substrate. However, due to possible adhesion energy variations and other unknown disturbances in the process, the peeling front could shift to a different location and v_p could vary. In an extreme case, the tensions t_1 and t_2 could align with each other, making the required tension force extremely large to peel the laminate. Therefore, the peeling process must be controlled to ensure the quality of transferred material.

2.1 Energy Release Rate in Roll-to-Roll Peeling. For the peeling process to be feasible, an energy balance condition must be satisfied between the energy release rate G of the peeling action and the adhesion energy Γ , i.e.,

$$G = \Gamma(\nu_p, \, \theta, \, \alpha) \tag{1}$$

Adhesion energy Γ quantifies the energy per unit area required to separate two bodies that are bonded by adhesion at the interface [42]. Consider an infinitesimal web section of length Δd_1 that is delaminated under tensions t_1 , t_2 , and t_3 with peeling angles θ_1 and θ_2 , as shown in Fig. 3. Denoting the unstretched length of Δd_1 as Δd , the energy dissipated due to the creation of the new interface area can be expressed as

$$U_1 = -\Gamma b \Delta d \tag{2}$$

where b is the width of the web.

During the peeling process, the potential energy of the system is increased due to the work done by the external forces t_2 and t_3 . When a free interface of unstretched length Δd is created, the released web sections are added to the two separated webs. While before delamination Δd is under tension t_1 , after delamination the released web sections are under tensions t_2 and t_3 , respectively. Based on the geometric relationship as shown in Fig. 3, the

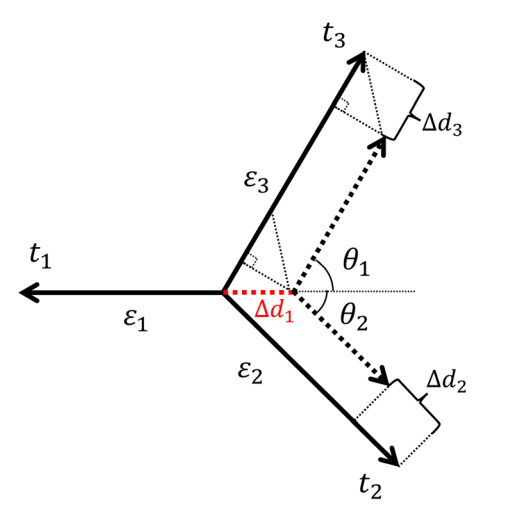


Fig. 3 Delamination (crack propagation) in the peeling process

distances that tensions t_2 and t_3 have traveled along their corresponding directions can be determined as

$$\Delta d_2 = \Delta d (1 - \cos \theta_2 + \varepsilon_2 - \varepsilon_1 \cdot \cos \theta_2) \tag{3}$$

$$\Delta d_3 = \Delta d(1 - \cos \theta_1 + \varepsilon_3 - \varepsilon_1 \cdot \cos \theta_1) \tag{4}$$

where ε_1 , ε_2 , and ε_3 are the strains in the three web sections and can be related to tension forces through $t_i = bh_{wi}E_i\varepsilon_i$. h_{wi} is the thickness and E_i is the elastic modulus of the corresponding web section i, i=1, 2, and 3. The unstretched web length Δd has a stretched length of $\Delta d_1 = \Delta d \cdot (1+\varepsilon_1)$ prior to delamination, and stretched lengths $\Delta d_2 = \Delta d \cdot (1+\varepsilon_2)$ and $\Delta d_3 = \Delta d \cdot (1+\varepsilon_3)$ after delamination. The work done by the tension forces to the system is thus obtained as

$$U_2 = t_2 \Delta d_2 + t_3 \Delta d_3 \tag{5}$$

Due to the strain change in the three web sections during the peeling process, the elastic potential energy of the system is also changed. According to Hooke's law, the elastic potential energy change during peeling is given by

$$U_3 = \frac{1}{2} V_2 E_2 \left(\varepsilon_1^2 - \varepsilon_2^2 \right) + \frac{1}{2} V_3 E_3 \left(\varepsilon_1^2 - \varepsilon_3^2 \right) \tag{6}$$

where V_2 and V_3 are the volumes of the unstreched upper and lower webs in the Δd section. Equation (6) can further be written as

$$U_3 = \frac{1}{2} E_2 b h_{w2} \Delta d \left(\varepsilon_1^2 - \varepsilon_2^2 \right) + \frac{1}{2} E_3 b h_{w3} \Delta d \left(\varepsilon_1^2 - \varepsilon_3^2 \right) \tag{7}$$

Based on energy conservation, the sum of U_1 , U_2 , and U_3 should be zero, i.e., $U_1 + U_2 + U_3 = 0$. Together with Eq. (1), this energy conservation condition yields the energy release rate as

$$G = \frac{t_3}{b} (1 - \cos \theta_1 + \varepsilon_3 - \varepsilon_1 \cdot \cos \theta_1)$$

$$+ \frac{t_2}{b} (1 - \cos \theta_2 + \varepsilon_2 - \varepsilon_1 \cdot \cos \theta_2) - \frac{h_{w3} \cdot E_3}{2} (\varepsilon_3^2 - \varepsilon_1^2)$$

$$- \frac{h_{w2} \cdot E_2}{2} (\varepsilon_2^2 - \varepsilon_1^2)$$
(8)

In a steady peeling process, a force balance is also achieved among t_1 , t_2 , and t_3 . This condition can be used to establish the following relations.

$$t_2 + t_3 \cos \theta + t_1 \cos \alpha = 0 \tag{9}$$

$$t_1 \sin \alpha = t_3 \sin \theta \tag{10}$$

where

$$\theta = \theta_1 + \theta_2 \tag{11}$$

$$\alpha = \pi - \theta_2 \tag{12}$$

Compared with traditional formulations based on adhesion mechanics, the above energy release rate model considers the R2R configuration, as well as the strain energy stored in the flexible substrates.

2.2 Roll-to-Roll Peeling Front Dynamics. Maintaining a stable peeling front is required for achieving desired transfer quality in the R2R peeling process. The energy release rate model needs to be integrated into an R2R peeling front dynamics model to establish the relationship among tension, peeling speed, roller speed, and torque inputs. Consider again the schematic shown in Fig. 2. The webs in the system can be divided into three control volumes, each defined as the web section starting from the peeling front to the tangential point of the corresponding unwinding or winding rollers. The web lengths in the control volumes are denoted as $L_1(t)$, $L_2(t)$, and $L_3(t)$. The web lengths change because the peeling front location could change during the peeling process. Assuming that the web in each control volume has a uniform strain, the unstretched web lengths can be obtained as:

$$l_i(t) = \frac{L_i(t)}{(1 + \varepsilon_i(t))} \tag{13}$$

The unstretched length of the web can be used as a measure of the mass within its control volume since the density of the web is homogeneous in each control volume. Based on the law of mass conservation, the mass flow equation can be expressed as

$$\dot{l}_1(t) = \frac{v_1(t) - v_p(t)}{1 + \varepsilon_1(t)} \tag{14}$$

$$\dot{l}_2(t) = \frac{v_p(t)}{1 + \varepsilon_1(t)} - \frac{v_2(t)}{1 + \varepsilon_2(t)}$$
(15)

$$\dot{l}_3(t) = \frac{v_p(t)}{1 + \varepsilon_1(t)} - \frac{v_3(t)}{1 + \varepsilon_3(t)}$$
(16)

The equation for control volume 1 shows that the in-flow mass is controlled by the unwinding roller speed v_1 and the out-flow mass is dictated by the peeling front velocity v_p . For control volumes 2 and 3, the in-flow mass is the web peeled at a speed of v_p , and the out-flow mass is controlled by the rewinding velocities v_2 and v_3 . During the R2R peeling process, the energy release rate G changes as the tension on each web changes. Peeling happens when Eq. (1) is satisfied. If G is less than Γ , there will be no peeling, which means that the peeling front velocity will be zero, i.e., $v_p = 0$ when $G < \Gamma$.

To determine v_p , the following geometric constraint also needs to be satisfied. As shown in Fig. 4, a complex plane can be constructed with the origin at the center of the lower guiding roller, and a vector loop is formed as

$$\overrightarrow{W_1} + \overrightarrow{W_2} + \overrightarrow{W_3} = \overrightarrow{W_4} \tag{17}$$

which can then be expanded into

$$\frac{R}{\cos(\theta_2/2)} \cdot e^{i \cdot \left(\frac{\pi - \theta_2(t)}{2} - \beta(t)\right)} + h(t) \cdot e^{i \cdot (\theta_1(t) - \beta(t))} - R \cdot e^{i \cdot (-\gamma(t))}$$

$$= 2R \cdot e^{i \cdot \frac{\pi}{2}} \tag{18}$$

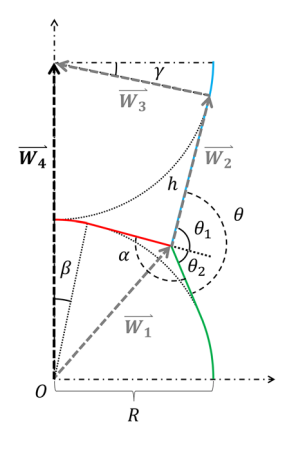


Fig. 4 Geometric constraint at the peeling front

where $\beta(t)$ is the angle that the incoming laminate is wrapped around the lower guiding roller, $\gamma(t)$ is the angle that the upper web is wrapped around the upper guiding roller, and h(t) is the web length between the peeling front and the tangential point on the upper roller.

In addition, the following equation holds according to the geometry shown in Fig. 4.

$$\beta(t) - \gamma(t) + \frac{\pi}{2} = \theta_1(t) \tag{19}$$

Furthermore, the lengths of the three webs within the peeling front area can be expressed as

$$L_1(t) - D_1 = R \cdot \beta(t) + R \cdot \tan\left(\frac{\theta_2(t)}{2}\right)$$
 (20)

$$L_2(t) - D_2 = R \cdot \left(\frac{\pi}{2} - \beta(t) - \theta_2(t)\right) + R \cdot \tan\left(\frac{\theta_2(t)}{2}\right)$$
 (21)

$$L_3(t) - D_3 = R \cdot \gamma(t) + h(t) \tag{22}$$

Note Eqs. (17)–(22) are defined based on the case $\theta_1(t) \ge \theta_2(t)$. Similar equations can be setup for the case $\theta_1(t) < \theta_2(t)$, since the configuration of the rollers is symmetrical.

The above peeling front dynamics model can be related to the torque inputs to the R2R dry transfer system through the following well-known roller dynamics model [43]:

$$v_1(t) = \omega_1(t) \cdot R_1 \tag{23}$$

$$\frac{J_2}{R_2} \cdot \dot{v_2}(t) = -t_2(t) \cdot R_2 + u_2(t) - \frac{f_2}{R_2} \cdot v_2(t)$$
 (24)

$$\frac{J_3}{R_3} \cdot \dot{v_3}(t) = -t_3(t) \cdot R_3 + u_3(t) - \frac{f_3}{R_3} \cdot v_3(t)$$
 (25)

where J_2 and J_3 are the rotational inertias of the rewinding rollers, f_2 and f_3 are friction coefficients of the rewinding roller and motor

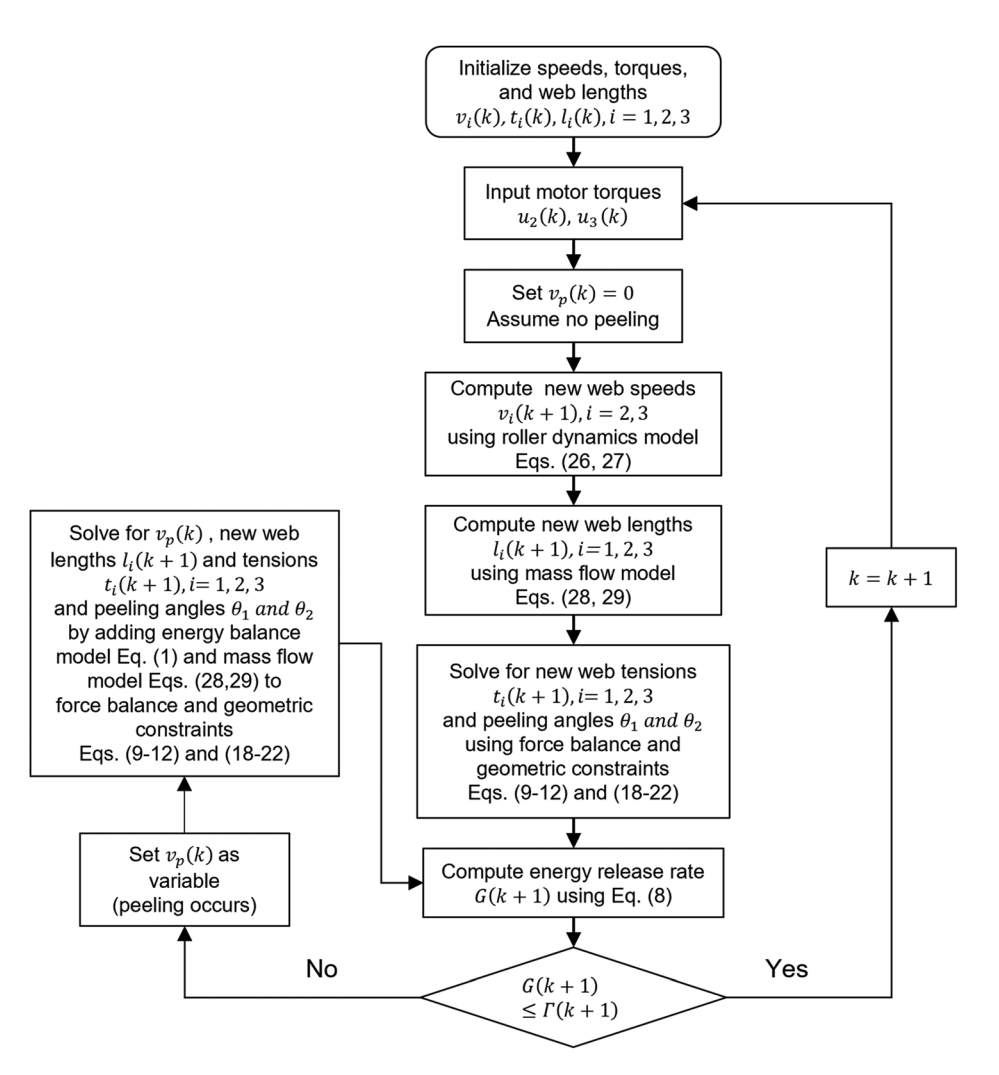


Fig. 5 A flowchart of the simulation procedure

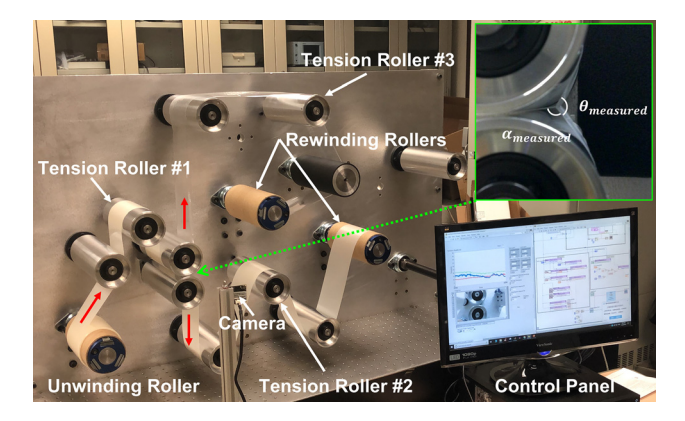


Fig. 6 Experimental setup

Table 1 System parameters

Parameters	Value				
E_1, E_2, E_3	2.7 GPa				
R, R_1, R_2, R_3	0.0381 m				
D_1	0.49 m				
D_2	1.02 m				
D_3	1.59 m				
h_{w2}, h_{w3}	$127 \mu m$				
b	0.1016 m				
J_2, J_3	$0.9511 \mathrm{kg} \mathrm{m}^2$				
f_2, f_3	$19.023\mathrm{N}\mathrm{m}\mathrm{s/rad}$				

assemblies, R_1 , R_2 , and R_3 are the radii of the unwinding and rewinding rollers, and u_2 and u_3 are the torque inputs to the two rewinding rollers.

2.3 Model Discretization and Simulation. Based on Eqs. (1)–(25), a simulation model is developed in MATLAB/Simulink to analyze the R2R peeling system. The roller velocity and the unstretched web length equations are discretized as

$$v_2(k+1) = v_2(k) + \frac{u_2(k) - t_2(k) \cdot R_2 - f_2 \cdot v_2(k) / R_2}{J_2} \cdot R_2 \cdot T_s$$
(26)

$$v_3(k+1) = v_3(k) + \frac{u_3(k) - t_3(k) \cdot R_3 - f_3 \cdot v_3(k) / R_3}{J_3} \cdot R_3 \cdot T_s$$
(27)

$$l_1(k+1) = l_1(k) + \frac{\left(v_1(k) - v_p(k)\right) \cdot T_s}{1 + \varepsilon_1(k)}$$
 (28)

$$l_i(k+1) = l_i(k) - \frac{v_i(k) \cdot T_s}{1 + \varepsilon_i(k)} + \frac{v_p(k) \cdot T_s}{1 + \varepsilon_i(k)}, \quad i = 2, 3$$
 (29)

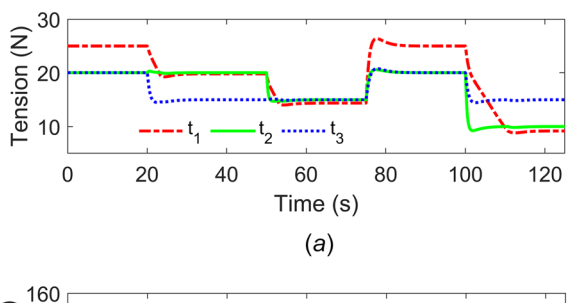
where k is the kth time-step and T_s is the sample interval of the simulation process. Figure 5 shows a flowchart of the simulation procedure. The simulation starts with a set of initial web speed, torque, and unstretched web length values. At each time-step, the peeling front velocity v_p is initially assumed zero, which means that there is no delamination occurring. For a given set of torque inputs $u_2(k)$ and $u_3(k)$, the simulation computes the new web speeds using Eqs. (26) and (27) and the new unstretched web lengths using Eqs. (28) and (29). The resulting tensions and peeling angles are determined by solving the force balance and geometric constraint equations, Eqs. (9)–(12) and (18)–(22). A new energy release rate G(k+1) is then calculated. If $G(k+1) \le \Gamma(k+1)$, v_p remains at zero and the simulation goes

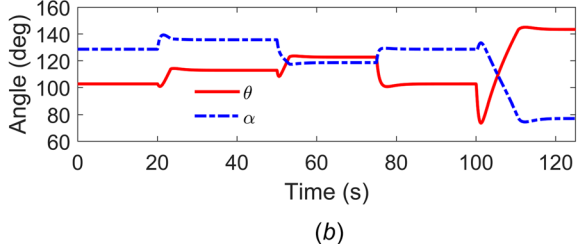
to the next time-step. If $G(k+1) > \Gamma(k+1)$, it means that there will be delamination occurring. Thus, there must exist a positive v_p that satisfies the energy balance equation, Eq. (1). This positive v_p can be solved together with the updated new web lengths, tensions, and peeling angles by solving the systems of equations Eqs. (1), (9)–(12), (12)–(22), (28), and (29).

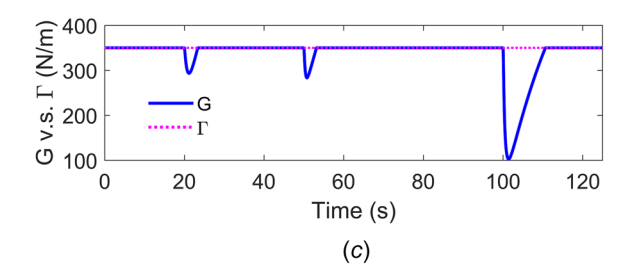
3 Experimental Setup

Experiments were conducted to validate the developed model based on a custom-built testbed as shown in Fig. 6. The unwinding roller was driven by a NEMA 23 stepper motor (1-DM542S-23HS45) and the rewinding rollers by two brushless servomotors (Aerotech BM130) with a 50:1 gearbox (PGCN23-5025). Three of the idler rollers were instrumented with load cells (MAGPOWR CL-1-50) to measure the web tensions. A digital camera was used to measure the peeling angle. The data acquisition and control algorithms were implemented using NI cRIO-9022. Two feedback controllers were implemented to track the tension setpoints of t_2 and t_3 independently. The web speed at the unwinding roller was controlled by the stepper motor.

Tension-controlled R2R peeling tests were conducted with two types of samples to validate the model under two different adhesion energy levels. The first sample was prepared by laminating







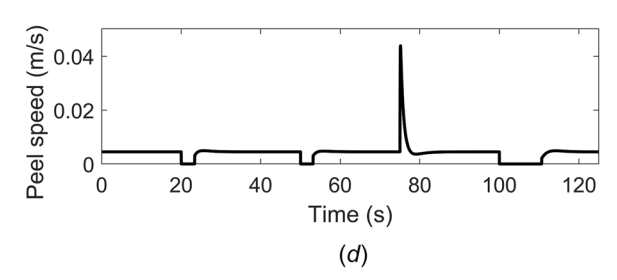


Fig. 7 Simulation results: (a) peeling tensions; (b) peeling angles; (c) estimated energy release rate and set adhesion energy; and (d) peeling front velocity v_p

two polyethylene terephthalate/ethylene vinyl acetate (PET/EVA) films (0.005 in. thick, 4 in. wide). The second sample was prepared by attaching Scotch tape (0.0023 in. thick, 2 in. wide) to the PET side of the PET/EVA film and the width of the PET/EVA film was trimmed to 2 in. wide. Table 1 provides a summary of relevant parameters used in the study. The roller inertias and friction coefficients are lumped parameters estimated using a system identification method based on the experimental setup.

4 Results and Discussion

Simulation Results. Numerical simulation was conducted to demonstrate that the developed model can capture the dynamics of the R2R peeling system. Figure 7 shows the simulation results from a case study that represents a typical R2R peeling process condition. The adhesion energy was set as a constant of 350 N/m and the unwinding roller speed v_1 at 0.45 cm/s. The tension settings of t_2 and t_3 were varied between 10 and 20 N, as shown in Fig. 7(a). The peeling tensions were initially set at $t_2 = t_3 = 20 \,\mathrm{N}$. At time = 20, 50, and 100 s, at least one of the peeling tensions was changed to a lower value, resulting in changed peeling angles as shown in Fig. 7(b). The calculated energy release rate is compared with the adhesion energy in Fig. 7(c). The peeling front velocity is shown in Fig. 7(d). The decreases in the peeling tensions caused the energy release rate to drop below the adhesion energy. As a result, the peeling front velocity v_p dropped to 0 m/s since the energy release rate was not high enough to propagate the peeling front. As the R2R process continued, the energy release rate increased while the peeling angles changed, moving the peeling front to a new location with a higher energy release rate. Peeling resumed when the energy release rate matched the adhesion energy again. At time = 75 s, the peeling front velocity increased dramatically, because the sudden increase of peeling tensions had resulted in a sudden increase of the strain energy. While the energy release rate must remain at the same level as the adhesion energy, the peeling front velocity v_p rapidly increased to absorb the sudden increase of the strain energy. When the tensions stabilized, the peeling front velocity returned to the same level as the unwinding speed. These simulation results matched well with our experimental observations and showed that the developed peeling system model could correctly capture the interaction among peeling tensions, angles, peeling front velocity, web speeds, and adhesion energy.

4.2 Experimental Results. Figure 8 shows a comparison between modeled and measured tension forces when peeling a PET/EVA sample. The peeling tensions t_2 and t_3 were first set at

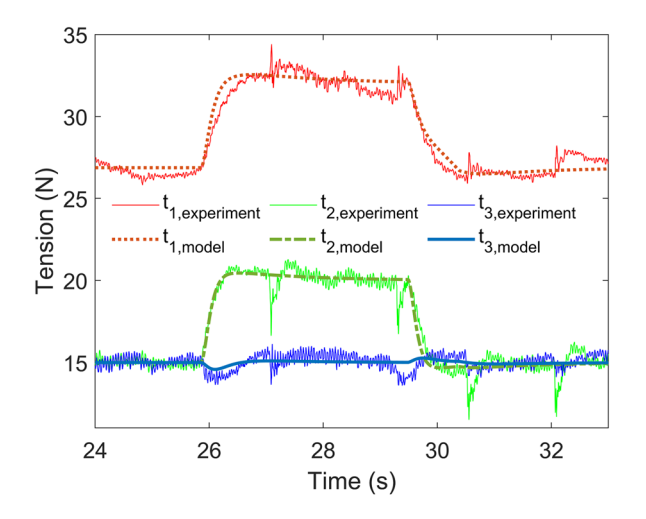


Fig. 8 Comparison between model-predicted and measured tension forces

15 N. These tension forces are achieved through torque control of the two rewinding rollers. The peeling tension t_2 was changed to 20 N at time = 25.8 s and later back to 15 N at time = 29.5 s. The peeling tension t_3 was maintained at 15 N all the time. As can be seen in the figure, the model-predicted and measured tension forces agreed very well. The transient response behavior of the tensions was due to the roller dynamics and the interaction between t_2 and t_3 in the peeling process. The noise observed on the measured tensions was caused by the bonding strength variation of the laminate sample, which was prepared manually, and it a uniform bonding strength was hard to achieve.

Figure 9 shows a comparison between the model-predicted and measured peeling angles with another PET/EVA sample. The web speed was set at 0.45 cm/s. As shown in Fig. 9(a), the peeling tensions t_2 and t_3 were initially maintained at 15 N, with a resulting t_1 at 25.5 N. Peeling tension t_3 was changed from 15 to 10 N at time = 174 s, causing t_1 to change accordingly. Then t_2 was changed to 10 N at time = 185 s. The peeling angles could not be measured in real-time with the current experimental setup; therefore, only three still images were taken and processed, as shown in Fig. 9(b). The measured peeling angles are compared with model-predicted ones at the corresponding moments when the three images were taken, as shown in Fig. 9(c).

Similar tests were conducted using Scotch tape laminate samples. Table 2 summarizes the predicted and measured peeling angles, as well as the estimated adhesion energy for both types of laminate samples. It shows that the predicted peeling angles agree well with the measured ones. It also shows that the estimated adhesion energy of the PET/EVA laminates is much lower than that of the Scotch tape laminates, suggesting that the developed peeling model can capture the effect of different adhesion energy levels. It should be noted that the adhesion energy in Table 2 was estimated based on the developed system model and measured peeling tensions. Since the energy release rate equals the adhesion

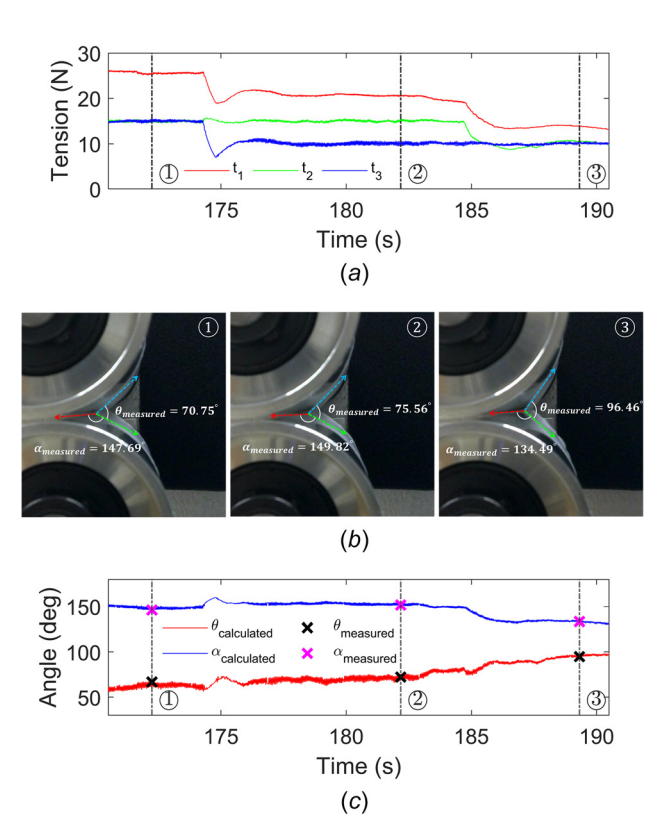


Fig. 9 Comparison between model-predicted and measured peeling angles: (a) tension measurements; (b) peeling front images and angle measurements; and (c) predicted and measured peeling angles

Table 2 Peeling experiment results

Sample	t_2 (N)	t ₃ (N)	t_1 (N)	$\theta_{\mathrm{predicted}}$ (°)	$\theta_{ m measured}$ (°)	θ_{error} (%)	$\alpha_{predicted} \; (^{\circ})$	$\alpha_{measured} \; (^{\circ})$	$\alpha_{error}\left(\%\right)$	Γ _{estimated} (N/m)
PET/EVA	15.31	15.32	25.53	67.08	70.75	5.19	146.45	147.69	0.84	50.20
PET/EVA	15.21	9.98	20.60	72.08	75.56	4.60	152.55	149.82	1.82	45.18
PET/EVA	10.38	10.15	13.89	94.88	96.46	1.64	133.26	134.49	0.91	65.35
PET/EVA	9.80	10.31	11.64	109.32	110.42	0.99	123.29	123.43	0.11	83.36
Tape on PET	15.09	15.13	12.68	130.39	133.51	2.33	114.64	112.41	1.98	345.28
Tape on PET	20.11	20.18	22.25	112.96	115.23	1.97	123.37	121.89	1.21	355.19
Tape on PET	24.92	26.27	30.69	106.38	107.67	1.20	124.80	128.48	2.86	403.54
Tape on PET	15.24	19.89	17.38	122.51	126.94	3.49	105.18	109.05	3.55	349.41

energy during a stable peeling process, the computed energy release rate while peeling occurs can be used as the adhesion energy of the laminate under those operating conditions.

Conclusion 5

A dynamic system model for an R2R peeling process is developed and demonstrated for dry transfer of 2D materials and printed electronics. The model integrates R2R peeling front dynamics and roller dynamics to predict the interaction among peeling process parameters, including adhesion energy, peeling angle, speed, and force. Numerical simulation and experiments were conducted to validate the model. It is shown that the model correctly captures the transient behavior of the peeling process and can be used for R2R peeling process simulation and control design. Future work will include to design a model-based controller for the R2R peeling process and to test the control system for large-scale dry transfer of chemical vapor deposition graphene.

Acknowledgment

This work is based upon work supported primarily by the National Science Foundation under Cooperative Agreement Nos. EEC-1160494 and CMMI-2041470. Any opinions, findings, and conclusions or recommendations expressed in this material are those of the author(s) and do not necessarily reflect the views of the National Science Foundation.

References

- [1] Unander, T., and Nilsson, H.-E., 2009, "Characterization of Printed Moisture Sensors in Packaging Surveillance Applications," IEEE Sens. J., 9(8), pp.
- [2] Kang, H., Park, H., Park, Y., Jung, M., Kim, B. C., Wallace, G., and Cho, G., 2015, "Fully Roll-to-Roll Gravure Printable Wireless (13.56 MHz) Sensor-Signage Tags for Smart Packaging," Sci. Rep., 4(1), p. 5387.
- [3] Subramanian, V., Chang, P. C., Lee, J. B., Molesa, S. E., and Volkman, S. K., 2005, "Printed Organic Transistors for Ultra-Low-Cost RFID Applications," IEEE Trans. Compon. Packag. Technol., 28(4), pp. 742-747.
- [4] Allen, M., Lee, C., Ahn, B., Kololuoma, T., Shin, K., and Ko, S., 2011, "R2R Gravure and Inkjet Printed RF Resonant Tag," Microelectron. Eng., 88(11), pp.
- [5] Kopola, P., Aernouts, T., Sliz, R., Guillerez, S., Ylikunnari, M., Cheyns, D., Välimäki, M., Tuomikoski, M., Hast, J., Jabbour, G., Myllylä, R., and Maaninen, A., 2011, "Gravure Printed Flexible Organic Photovoltaic Modules," Sol. Energy Mater. Sol. Cells, 95(5), pp. 1344–1347.
- [6] Krebs, F. C., Gevorgyan, S. A., and Alstrup, J., 2009, "A Roll-to-Roll Process to Flexible Polymer Solar Cells: Model Studies, Manufacture and Operational Stability Studies," J. Mater. Chem., 19(30), pp. 5442-5451.
- [7] Søndergaard, R., Hösel, M., Angmo, D., Larsen-Olsen, T. T., and Krebs, F. C., 2012, "Roll-to-Roll Fabrication of Polymer Solar Cells," 15(1-2), pp. 36-49.
- [8] Noh, J., Yeom, D., Lim, C., Cha, H., Han, J., Kim, J., Park, Y., Subramanian, V., and Cho, G., 2010, "Scalability of Roll-to-Roll Gravure-Printed Electrodes on Plastic Foils," IEEE Trans. Electron. Packag. Manuf., 33(4), pp. 275–283.
 [9] Gregg, A., York, L., and Strnad, M., 2005, "Roll-to-Roll Manufacturing of Flexible Displays," Flexible Flat Panel Disp., 3, p. 409.
- [10] van den Brand, J., De Baets, J., Van Mol, T., and Dietzel, A., 2008, "Systemsin-Foil-Devices, Fabrication Processes and Reliability Issues," Microelectron. Reliab., 48(8-9), pp. 1123-1128.
- [11] Xin, H., and Li, W., 2018, "A Review on High Throughput Roll-to-Roll Manufacturing of Chemical Vapor Deposition Graphene," Appl. Phys. Rev., 5(3), p. 031105.

- [12] Khan, S., Lorenzelli, L., and Dahiya, R. S., 2015, "Technologies for Printing Sensors and Electronics Over Large Flexible Substrates: A Review," IEEE Sens. J., 15(6), pp. 3164–3185.
- [13] Yang, S. Y., Carlson, A., Cheng, H., Yu, Q., Ahmed, N., Wu, J., Kim, S., Sitti, M., Ferreira, P. M., Huang, Y., and Rogers, J. A., 2012, "Elastomer Surfaces With Directionally Dependent Adhesion Strength and Their Use in Transfer Printing With Continuous Roll-to-Roll Applications," Adv. Mater., 24(16), pp. 2117-2122.
- [14] Li, X., Zhu, Y., Cai, W., Borysiak, M., Han, B., Chen, D., Piner, R. D., Colombo, L., and Ruoff, R. S., 2009, "Transfer of Large-Area Graphene Films for High-Performance Transparent Conductive Electrodes," Nano Lett., 9(12), pp. 4359–4363.
- [15] Pollard, B., 2011, Growing Graphene Via Chemical Vapor Deposition, Pomona College, Claremont, CA.
- [16] Zhang, Y., Zhang, L., and Zhou, C., 2013, "Review of Chemical Vapor Deposition of Graphene and Related Applications," Acc. Chem. Res., 46(10), pp.
- [17] Mattevi, C., Kim, H., and Chhowalla, M., 2011, "A Review of Chemical Vapour Deposition of Graphene on Copper," J. Mater. Chem., 21(10), pp. 3324-3334.
- [18] Hesjedal, T., 2011, "Continuous Roll-to-Roll Growth of Graphene Films by Chemical Vapor Deposition," Appl. Phys. Lett., 98(13), p. 133106.
- [19] Kobayashi, T., Bando, M., Kimura, N., Shimizu, K., Kadono, K., Umezu, N., Miyahara, K., Hayazaki, S., Nagai, S., Mizuguchi, Y., Murakami, Y., and Hobara, D., 2013, "Production of a 100-m-Long High-Quality Graphene Transparent Conductive Film by Roll-to-Roll Vapor Deposition and Transfer Process," Appl. Phys. Lett., 102(2), p. 023112.
- [20] Polsen, E. S., McNerny, D. Q., Viswanath, B., Pattinson, S. W., and Hart, A. J., 2015, "High-Speed Roll-to-Roll Manufacturing of Graphene Using a Concentric Tube CVD Reactor," Sci. Rep., 5(1), p. 10257.
- Yamada, T., Ishihara, M., Kim, J., Hasegawa, M., and Iijima, S., 2012, "A Rollto-Roll Microwave Plasma Chemical Vapor Deposition Process for the Production of 294 mm Width Graphene Films at Low Temperature," Carbon, 50(7), pp. 2615-2619.
- Yamada, T., Ishihara, M., and Hasegawa, M., 2013, "Large Area Coating of Graphene at Low Temperature Using a Roll-to-Roll Microwave Plasma Chemical Vapor Deposition," Thin Solid Films, 532, pp. 89–93.
- [23] Lee, B., Chu, W., and Li, W., 2020, "Effects of Process Parameters on Graphene Growth Via Low-Pressure Chemical Vapor Deposition," ASME J. Micro Nano-Manuf., 8(3), p. 031005.
- [24] Bae, S., Kim, H., Lee, Y., Xu, X., Park, J.-S., Zheng, Y., Balakrishnan, J., Lei, T., Kim, H. R., Song, Y. I., Kim, Y.-J., Kim, K. S., Özyilmaz, B., Ahn, J.-H., Hong, B. H., and Iijima, S., 2010, "Roll-to-Roll Production of 30-Inch Graphene Films for Transparent Electrodes," Nat. Nanotechnol., 5(8), pp.
- [25] Deng, B., Hsu, P.-C., Chen, G., Chandrashekar, B. N., Liao, L., Ayitimuda, Z., Wu, J., Guo, Y., Lin, L., Zhou, Y., Aisijiang, M., Xie, Q., Cui, Y., Liu, Z., and Peng, H., 2015, "Roll-to-Roll Encapsulation of Metal Nanowires Between Graphene and Plastic Substrate for High-Performance Flexible Transparent Electrodes," Nano Lett., 15(6), pp. 4206-4213.
- [26] Chandrashekar, B. N., Deng, B., Smitha, A. S., Chen, Y., Tan, C., Zhang, H., Peng, H., and Liu, Z., 2015, "Roll-to-Roll Green Transfer of CVD Graphene Onto Plastic for a Transparent and Flexible Triboelectric Nanogenerator," Adv. Mater., 27(35), pp. 5210-5216.
- [27] Xin, H., Zhao, Q., Chen, D., and Li, W., 2018, "Roll-to-Roll Mechanical Peeling for Dry Transfer of Chemical Vapor Deposition Graphene," ASME J. Micro Nano-Manuf., 6(3), p. 031004.
- [28] Zhao, Q., Hong, N., Chen, D., and Li, W., 2020, "Controlling Peeling Front Geometry in a Roll-to-Roll Thin Film Transfer Process," ASME Paper No. MSEC2020-8507.
- [29] Linghu, C., Zhang, S., Wang, C., and Song, J., 2018, "Transfer Printing Techniques for Flexible and Stretchable Inorganic Electronics," npj Flexible Electron., 2(1), 26.
- [30] Hong, N., Kireev, D., Zhao, O., Chen, D., Akinwande, D., and Li, W., 2021. "Roll-to-Roll Dry Transfer of Large-Scale Graphene," Adv. Mater., 34(3),
- [31] Kendall, K., 1975, "Thin-Film Peeling-the Elastic Term," J. Phys. D, 8(13), pp. 1449-1452.

- [32] Gao, E., Lin, S.-Z., Qin, Z., Buehler, M. J., Feng, X.-Q., and Xu, Z., 2018, "Mechanical Exfoliation of Two-Dimensional Materials," J. Mech. Phys. Solids, 115, pp. 248–262.
- [33] Huang, Y., Liu, H., Xu, Z., Chen, J., and Yin, Z., 2018, "Conformal Peeling of Device-on-Substrate System in Flexible Electronic Assembly," IEEE Trans. Compon., Packag. Manuf. Technol., 8(8), pp. 1496–1506.
- Compon., Packag. Manuf. Technol., 8(8), pp. 1496–1506.

 [34] Wie, D. S., Zhang, Y., Kim, M. K., Kim, B., Park, S., Kim, Y.-J., Irazoqui, P. P., Zheng, X., Xu, B., and Lee, C. H., 2018, "Wafer-Recyclable, Environment-Friendly Transfer Printing for Large-Scale Thin-Film Nanoelectronics," Proc. Natl. Acad. Sci., 115(31), pp. E7236–E7244.
- [35] Yoo, B., Cho, S., Seo, S., and Lee, J., 2014, "Elastomeric Angled Microflaps With Reversible Adhesion for Transfer-Printing Semiconductor Membranes Onto Dry Surfaces," ACS Appl. Mater. Interfaces, 6(21), pp. 19247–19253.
 [36] Ghareeb, A., and Elbanna, A., 2019, "Adhesion Asymmetry in Peeling of Thin
- [36] Ghareeb, A., and Elbanna, A., 2019, "Adhesion Asymmetry in Peeling of Thin Films With Homogeneous Material Properties: A Geometry-Inspired Design Paradigm," ASME J. Appl. Mech., 86(7), p. 071005.
- [37] Kovalchick, C., Molinari, A., and Ravichandran, G., 2014, "Rate Dependent Adhesion Energy and Nonsteady Peeling of Inextensible Tapes," ASME J. Appl. Mech., 81(4), p. 041016.

- [38] Peng, Z., Wang, C., Chen, L., and Chen, S., 2014, "Peeling Behavior of a Viscoelastic Thin-Film on a Rigid Substrate," Int. J. Solids Struct., 51(25–26), pp. 4596–4603.
- [39] Perrin, H., Eddi, A., Karpitschka, S., Snoeijer, J. H., and Andreotti, B., 2019, "Peeling an Elastic Film From a Soft Viscoelastic Adhesive: Experiments and Scaling Laws," Soft Matter, 15(4), pp. 770–778.
- [40] Dalbe, M.-J., Villey, R., Ciccotti, M., Santucci, S., Cortet, P.-P., and Vanel, L., 2016, "Inertial and Stick-Slip Regimes of Unstable Adhesive Tape Peeling," Soft Matter, 12(20), pp. 4537–4548.
- [41] Villey, R., Creton, C., Cortet, P.-P., Dalbe, M.-J., Jet, T., Saintyves, B., Santucci, S., Vanel, L., Yarusso, D. J., and Ciccotti, M., 2015, "Rate-Dependent Elastic Hysteresis During the Peeling of Pressure Sensitive Adhesives," Soft Matter, 11(17), pp. 3480–3491.
- [42] Xin, H., Borduin, R., Jiang, W., Liechti, K. M., and Li, W., 2017, "Adhesion Energy of as-Grown Graphene on Copper Foil With a Blister Test," Carbon, 123, pp. 243–249.
- [43] Pagilla, P. R., Siraskar, N. B., and Dwivedula, R. V., 2007, "Decentralized Control of Web Processing Lines," IEEE Trans. Control Syst. Technol., 15(1), pp. 106–117.